Spectroscopic Characterization of the Soluble Guanylate Cyclase-like Heme Domains from *Vibrio cholerae* and *Thermoanaerobacter tengcongensis*†

David S. Karow,‡ Duohai Pan,§,|| Rosalie Tran,§ Patricia Pellicena,⊥ Andrew Presley,§ Richard A. Mathies,§,# and Michael A. Marletta*,§,⊥,#

Program in Cellular and Molecular Biology, University of Michigan, Ann Arbor, Michigan 48109, and Department of Chemistry, Department of Molecular and Cell Biology, and Division of Physical Biosciences, Lawrence Berkeley Laboratory, University of California, Berkeley, California 94720

Received March 31, 2004; Revised Manuscript Received May 28, 2004

ABSTRACT: Soluble guanylate cyclase (sGC) is a nitric oxide- (NO-) sensing hemoprotein that has been found in eukaryotes from *Drosophila* to humans. Prokaryotic proteins with significant homology to the heme domain of sGC have recently been identified through genomic analysis. Characterization of two of these proteins is reported here. The first is a 181 amino acid protein cloned from *Vibrio cholerae* (VCA0720) that is encoded in a histidine kinase-containing operon. The ferrous unligated form of VCA0720 is 5-coordinate, high-spin. The CO complex is low-spin, 6-coordinate, and the NO complex is high-spin and 5-coordinate. These ligand-binding properties are very similar to those of sGC. The second protein is the N-terminal 188 amino acids of Tar4 (*Tt*Tar4H), a predicted methyl-accepting chemotaxis protein (MCP) from the strict anaerobe *Thermoanaerobacter tengcongensis*. *Tt*Tar4H forms a low-spin, 6-coordinate ferrous−oxy complex, the first of this sGC-related family that binds O_2. *Tt*Tar4H has ligand-binding properties similar to those of the heme-containing O_2 sensors such as *Ax*PDEA1. sGC does not bind O_2 despite having a porphyrin with a histidyl ligand like the globins. The results reported here, with sequence-related proteins from prokaryotes but in the same family as the sGC heme domain, show that these proteins have evolved to discriminate between ligands such as NO and O_2; hence, we term this family H−NOX domains (*h*eme−*n*itric oxide/*ox*ygen).

One important function of hemoproteins is to sense gaseous, diatomic small molecules (*1*). There are four distinct heme-binding domains that have been found in heme-based sensors. They can be segregated on the basis of their ligand specificity, functioning to sense either O_2, CO, or NO. There are two domains that are specialized for O_2 sensing, both found in prokaryotes. The first is the Mb- (myoglobin-) like heme domain that is contained within HemAT (*2*, *3*), an aerotaxis-regulating protein, and the second is the heme−PAS domain, which is found in the histidine kinase-containing protein, FixL (*4*, *5*), and the phosphodiesterase-containing *Ax*PDEA1 protein from *Acetobacter xylinum* (*6*). The third domain functions to sense CO and is found in the *Rhodospirillum rubrum* CooA protein. CooA regulates genes involved in CO oxidation (*7*). Finally, the last domain is specialized for NO binding and is found in the NO-responsive soluble guanylate cyclase (sGC).[1] This enzyme, found in many animals, has a heme-containing N-terminus that binds NO, regulating a C-terminal guanylate cyclase (*8*). sGC catalyzes the conversion of GTP to cGMP and is a heterodimer, composed of α and β subunits. Nitric oxide binds to the ferrous heme, which is ligated to the β subunit (*9*), and stimulates the activity of the enzyme over 200-fold (*10*). sGC has been characterized in eukaryotes ranging from *Drosophila* to humans; however, no sGCs or sGC-like proteins have been characterized in prokaryotes.

Recently, a PSI-BLAST search with the sGC heme domain as the query sequence identified multiple, predicted prokaryotic proteins with homology to this region (*11*); however, no further analysis was performed. We have now cloned and characterized two of these proteins: a 181 amino acid protein from *Vibrio cholerae* (VCA0720) and the heme domain (188 amino acids) from the *Thermoanaerobacter tengcongenesis* Tar4 protein (*Tt*Tar4H). These proteins share spectroscopic properties, sequence homology, and key conserved residues with sGC, and therefore, we place them in the same family. Although conserved from prokaryotes to humans, the biological role for these sGC-like heme domains has likely

† This work was supported in part by LDRD funds from the Lawrence Berkeley National Laboratory (M.A.M.).

* To whom correspondence should be addressed at the Department of Chemistry, University of California, Berkeley. Telephone: 510-643-9325. Fax: 510-643-9388. E-mail: marletta@berkeley.edu.

‡ Program in Cellular and Molecular Biology, University of Michigan.

§ Department of Chemistry, University of California, Berkeley.

|| Present address: Pacific Northwest National Laboratory, K8-88, Richland, WA 99352.

⊥ Department of Molecular and Cell Biology, University of California, Berkeley.

Division of Physical Biosciences, Lawrence Berkeley Laboratory, University of California, Berkeley.

[1] Abbreviations: sGC, soluble guanylate cyclase; *Tt*Tar4H, residues 1−188 of *Thermoanaerobacter tengcongensis* Tar4 (heme domain); MCP, methyl-accepting chemotaxis protein; AxPDEA1H, *Acetobacter xylinum* phosphodiesterase A1 heme domain; Mb, myoglobin; H−NOX domain, *h*eme−*n*itric oxide/*ox*ygen binding domain; DTT, dithiothreitol; DEA, diethylamine; TEA, triethylamine.

10.1021/bi049374l CCC: $27.50
Published on Web 07/13/2004

diverged, evidenced by the observation that it is contained in a histidine kinase containing operon in *V. cholerae*, a MCP in *T. tengcongensis*, and guanylate cyclases in eukaryotes.

Consistent with different functions, these proteins have very different ligand-binding properties. For example, as shown by resonance Raman and UV/vis spectroscopy, VCA0720 has ligand-binding characteristics essentially identical to those of sGC, while, strikingly, *Tt*Tar4H is able to bind O_2 and has ligand-binding characteristics most similar to those of Mb and known O_2 sensors such as FixL and *Ax*PDEA1. These spectroscopic results suggest that with the appropriate amino acid substitutions the sGC-like heme domain can discriminate between NO and O_2; hence, we term the proteins in this family H−NOX domains (*h*eme−*n*itric oxide/*ox*ygen).

MATERIALS AND METHODS

Construction of Expression Plasmids. PCR was used to amplify *Tt*Tar4H [1−564 bp of TTE0680 (Tar4)] and VCA0720 from *T. tengcongensis* and *V. cholerae* genomic DNA (ATCC), respectively, using Expand polymerase (Roche). The upstream primers were 5′-ggaattccatatgcaaggcattatctataccgttctc-3′ and 5′-ggaattccatatgaaggggacaatcgtcgggacatgg-3′ for VCA0720 and *Tt*Tar4H, respectively. The predicted VCA0720 protein sequence contained ten N-terminal amino acids that were not homologous to the other predicted H−NOX domains, and thus, the 5′ end of the upstream primer corresponded to the Met residue that precedes Gln-Gly-Ile (M11). The downstream primers were 5′-atagtttagcggccgctcatgatggcaaaaattccactac-3′ and 5′-atagtttagcggccgctcaatttttcttatactcaaaaacgggg-3′ for VCA0720 and *Tt*Tar4H, respectively. Upstream and downstream primers (Qiagen) contained *Nde*I and *Not*I restriction sites, respectively. Amplified PCR products were cloned into pET-20b (Novagen) and sequenced (UC Berkeley sequencing core and Elim Biopharmaceuticals, Inc.).

Escherichia coli Expression. Expressions were performed as described previously (*12*) with the following modifications. Plasmids were transformed into Tuner DE3 plysS cells (Novagen). Cultures were grown until an OD_{600} of 0.5−1 and cooled to 27 °C. Isopropyl β-D-thiogalactopyranoside (Promega) was added to 10 μM and aminolevulinic acid to 1 mM. Cultures were grown overnight for 14−18 h and then harvested.

Protein Purification. VCA0720 was purified in the following manner: Frozen cell pellets from 3 L of culture were thawed quickly at 37 °C and resuspended in 120 mL of buffer A [50 mM DEA, pH 8.5, 20 mM NaCl, 5 mM DTT, 1 mM Pefabloc (Pentapharm) ,and 5% glycerol]. Resuspended cells were lysed with sonication and, subsequently, with an Emulsiflex-C5 high-pressure homogenizer at 20000 psi (Avestin, Inc.). Lysed cells were centrifuged at 100000*g* for 40 min. The supernatant was applied to a 100 mL (2.5 × 21 cm) Toyopearl Q 650M anion-exchange column (Tosohaas), washed with 3 column volumes of buffer A, and developed with a linear NaCl gradient from 20 to 500 mM (800 mL). The flow rate was 1.5 mL/min for loading and 1 mL/min for washing and eluting. Fractions were selected on the basis of the intensity of the red/brown color. The eluate (∼50 mL) was concentrated to 4 mL using 15 mL 10K MWCO spin concentrators (Millipore). The concentrated proteins were applied to a prepacked Superdex S200 HiLoad 26/60 gel filtration column (Pharmacia) that had been equilibrated with TEA, pH 7.5, 50 mM NaCl, 5mM DTT, and 5% glycerol. The flow rate was 1.3 mL/min. Fractions containing VCA0720 were pooled and applied to a POROS HQ 7.9 mL (1 × 10 cm, 10 μm) anion-exchange column (Applied Biosystems) at 10 mL/min that had been equilibrated with buffer B (50 mM DEA, pH 8.5, 50 mM NaCl, and 5% glycerol). The column was washed with 3 column volumes of buffer B at 10 mL/min and developed with a linear gradient of NaCl from 50 to 500 mM in a total volume of 140 mL at the same flow rate. VCA0720-containing fractions were pooled and stored at −70 °C.

*Tt*Tar4H was lysed in buffer A as described above for VCA0720. The supernatant was subjected to heat denaturation (75 °C for 40 min) and centrifuged at 100000*g* for 40 min. The supernatant was applied to the same Toyopearl Q column used for VCA0720. This column had been equilibrated with buffer A, and the flow-through was collected. The *Tt*Tar4H-containing flow-through was concentrated to 4 mL and subjected to gel filtration as described above for VCA0720 except that the buffer contained 50 mM TEA, pH 7.4, 200 mM NaCl, and 5% glycerol. *Tt*Tar4H-containing fractions were pooled and stored at −70 °C.

UV/Vis Spectroscopy. All spectra were recorded in an anaerobic cuvette on a Cary 3E spectrophotometer equipped with a Neslab RTE-100 temperature controller set at 10 °C. Spectra were recorded from proteins in a solution of 50 mM TEA, pH 7.5, and 50 mM NaCl (buffer C). The heme concentration was ∼5 μM. Protein samples were placed into the anaerobic cuvette in an anaerobic glovebag (Coy) except for the $Fe^{2+}-O_2$ *Tt*Tar4H complex. Fe^{2+}-unligated protein samples were prepared in the following manner: Purified protein was made anaerobic in an O_2-scavenged gas manifold with 10 cycles of alternate evacuation and purging with purified argon and brought into an anaerobic glovebag. For *Tt*Tar4H, ferricyanide (∼100 equiv) was added to remove the bound O_2. Ferricyanide was removed using a PD10 desalting column (Amersham Biosciences) that had been equilibrated with buffer C, and then the protein was reduced using dithionite (∼100 equiv). The dithionite was then removed in the same manner. For consistency, VCA0720 was prepared in the same manner. The CO complexes were generated by adding Fe^{2+}-unligated protein to a sealed Reacti-Vial (Pierce) that contained CO (Airgas). NO complexes were generated by preparing an anaerobic solution of diethylamine NONOate (Caymen) in buffer C (∼10 mM) in a sealed Reacti-Vial. The headspace (1 mL) was then removed using a gastight syringe and delivered to an Fe^{2+}-unligated protein sample contained in a sealed Reacti-Vial. Lastly, $Fe^{2+}-O_2$ *Tt*Tar4H was formed by removing Fe^{2+}-unligated *Tt*Tar4H from the anaerobic chamber and exposing to air.

Extinction Coefficient Determination. An anaerobic, Fe^{2+}-unligated, UV/vis spectrum was recorded for both protein samples. These samples, along with the Mb standard, were prepared by oxidizing and rereducing each sample anaerobically as described above. The heme concentration was then determined for each sample by HPLC (*13*) and used to determine the Fe^{2+}-unligated extinction coefficient. This extinction coefficient was then used to determine the heme concentration and extinction coefficients for the CO, NO,

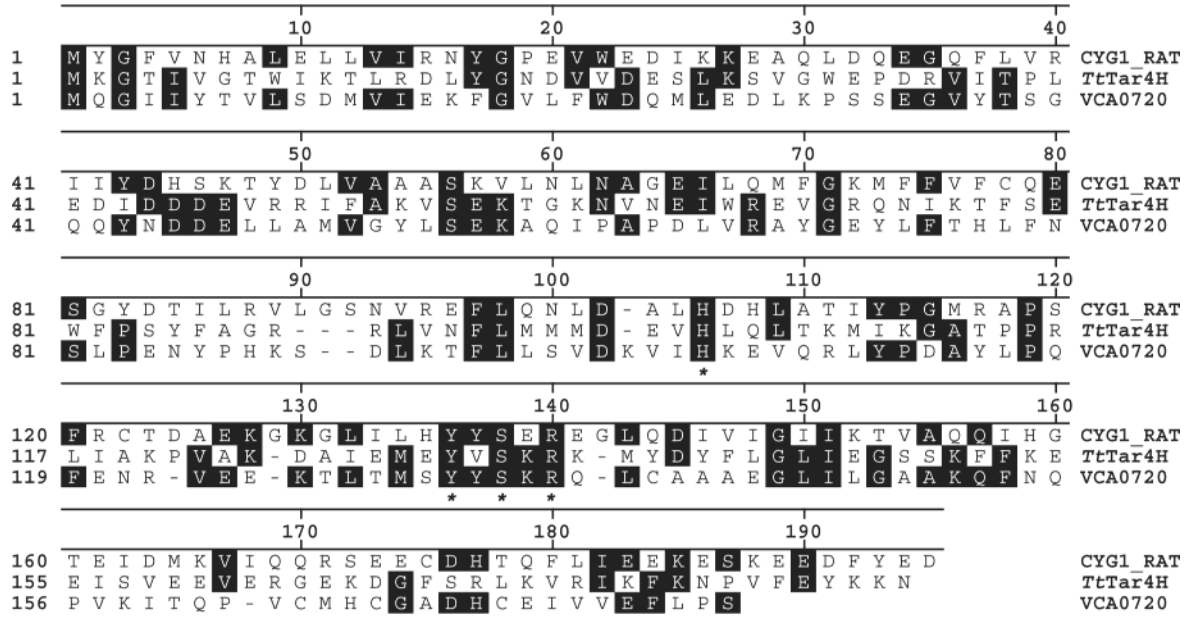

FIGURE 1: Alignment of rat β1(1−194) (CYG1_RAT) with *Tt*Tar4H and VCA0720. The alignment was generated using DNASTAR's Megalign program and the Clustal W algorithm. Conserved residues that are identical to the consensus sequence are shaded in black. Specific residues discussed in the text are marked with an asterisk (His105, the heme ligand, and Tyr135, Ser137, and Arg139 using the rat β1 numbering).

and $Fe^{2+}-O_2$ complexes from previously recorded UV/vis spectra. The HPLC method used to determine the heme concentration was performed with a protein C4 column (250 × 4.6 mm, 5 μm; Vydac) and a Hewlett-Packard Series II 1090 HPLC with a diode array detector. Each sample (25 μL) was applied to the C4 column that had been equilibrated with 0.1% trifluoroacetic acid (TFA). The column was developed with a linear gradient of 0−75% acetonitrile over 15 min followed by a linear gradient of 75−95% acetonitrile over 5 min. The flow rate was 1 mL/min.

Resonance Raman Spectroscopy. Spectra of all samples were collected using 413.1 nm excitation from a krypton ion laser (Spectra-Physics 2025), except for the VCA0720 NO complex, which was excited at 406.7 nm. A microspinning sample cell was used to minimize photoinduced degradation. Raman scattering was detected with a cooled, back-illuminated CCD (LN/CCD-1100/PB; Roper Scientific) controlled by a ST-133 controller coupled to a subtractive dispersion, double spectrograph (*14*). Raman spectra were corrected for the wavelength dependence of the spectrometer efficiency by using a white lamp and calibrated with cyclohexane. The reported frequencies are accurate to ±2 cm^{-1}, and the resolution of the spectra is 8 cm^{-1}. All Raman spectra were obtained by subtracting the buffer background and baseline correction. The laser power at the sample was 3 mW, except for the CO complexes where a power of 0.2 mW was used to avoid photolysis. Typical data acquisition times were 30 min. Absorption spectra taken pre- and post-Raman spectral collection confirmed the integrity of the ferrous unligated−*Tt*Tar4H and NO−*Tt*Tar4H samples. Approximate isotopic shifts were estimated on the basis of a simple diatomic harmonic oscillator model.

Protein samples were placed into the Raman cell in an anaerobic glovebag except for the $Fe^{2+}-{}^{16}O_2$ *Tt*Tar4H complex. The heme concentration was 17 μM for VCA0720 and 47 μM for *Tt*Tar4H. Protein samples for Raman spectroscopy were prepared as described above for UV/vis spectroscopy with the following modifications. ^{13}CO (99% containing ~10% $^{18}O_2$; Cambridge Isotopes) and $^{18}O_2$ (Spectra Gases) complexes were prepared in a manner similar to that of the ^{12}CO complexes. ^{15}NO complexes were made in the following manner: A 1 mL solution of 0.5 M $K^{15}NO_2$ (Cambridge Isotopes) and a 1 mL solution of 1 M KI/H_2SO_4 were made anaerobic on an oxygen-scavenged gas manifold and delivered into the anaerobic glovebag. A potassium nitrite solution (100 μL) was delivered to the KI solution using a gastight syringe. ^{15}NO-containing headspace (~1 mL) was then delivered to a protein sample contained in a sealed Reacti-Vial.

RESULTS

Cloning, Expression, and Purification. The predicted 181 amino acid ORF from *V. cholerae* (VCA0720) is encoded within a predicted histidine kinase-containing operon and is 22% identical to rat β1(1−194). The N-terminal sGC-like heme domain region from *T. tengcongensis* was identified in the Tar4 protein, a predicted MCP. The heme domain of this protein was assumed to extend from residue 1 to residue 188, the last amino acid before the predicted membrane-spanning region. This sGC-like heme domain is 18% identical to rat β1(1−194). An alignment of these two proteins with β1(1−194) is shown in Figure 1. These two proteins were cloned and expressed in *E. coli* and purified as described in Materials and Methods. Purity was assessed by Coomassie staining of samples resolved by SDS−PAGE (data not shown). Except for minor contaminating bands, the proteins were pure. The yield was ~6 and 20 mg/L for VCA0720 and *Tt*Tar4H, respectively. *Tt*Tar4H was isolated as the $Fe^{2+}-O_2$ complex (Soret maximum at 416 nm), and VCA0720 was isolated with a Soret maximum at 423 nm and a split α/β region (data not shown). It was assumed that the VCA0720 sample was a mixture of ferrous and ferric oxidation states and was not further characterized. Upon reduction with dithionite, the isolated VCA0720 formed a

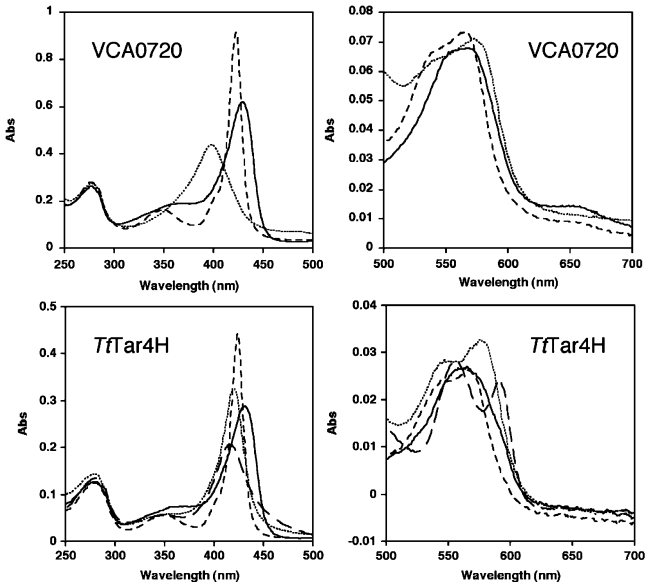

FIGURE 2: Electronic absorption spectra of VCA0720 and *Tt*Tar4H showing the Soret maximum and α/β region: reduced, unligated (—); CO complex (- - -); NO complex (• • •); and O_2 complex (— —). The heme concentration was ~5 μM.

Table 1: UV/Vis Peak Positions[a] and Extinction Coefficients[b]

protein	Soret	β	α	ref
sGC	431 (111)	555 (14)		*10*
VCA0720	429 (137)	568 (15.0)		this work
*Tt*Tar4H	431 (124)	565 (11.6)		this work
Hb	430 (133)	555 (12.5)		*15*
CO bound				
sGC	423 (145)	541 (14)	567 (14)	*10*
VCA0720	423 (203)	541 (14.9)	566 (16.3)	this work
*Tt*Tar4H	424 (191)	544 (10.3)	565 (11.3)	this work
Hb	419 (191)	540 (13.4)	569 (13.4)	*15*
NO bound				
sGC	398 (79)	537 (12)	572 (12)	*10*
VCA0720	398 (97)	540 (14.1)	573 (15.7)	this work
*Tt*Tar4H	420 (140)	547 (12.2)	575 (14.0)	this work
Hb	418 (130)	545 (12.6)	575 (13.0)	*15*
O_2 bound				
*Tt*Tar4H	416 (89)	556 (12.2)	591 (10.4)	this work
Hb	415 (125)	541 (13.5)	576 (14.6)	*15*

[a] In nm. [b] In mM^{-1} cm^{-1}.

high-spin, 5-coordinate ferrous complex. UV/vis and resonance Raman spectroscopy were then used to characterize the heme environment and ligand-binding characteristics of both proteins.

UV/Vis Absorption Spectroscopy. UV/vis spectra are shown in Figure 2, and the data with extinction coefficients are summarized in Table 1 and compared to sGC (*10*) and hemoglobin (*15*).

(A) Fe^{2+}-Unligated and CO Complexes. Both of these proteins have spectra that are similar to one another. The Fe^{2+}-unligated spectra exhibit Soret bands at ~431 nm and single, broad α/β bands at ~560 nm. Addition of CO to the anaerobically reduced proteins resulted in CO complexes with sharp Soret bands at ~424 nm, increases in the extinction coefficient, and split α/β bands. The shape and absorption maxima of the Soret and α/β bands for both the Fe^{2+}-unligated and CO complexes are very similar to those of full-length sGC, suggesting that the reduced proteins are 5-coordinate, high-spin and the CO complexes are 6-coordinate, low-spin.

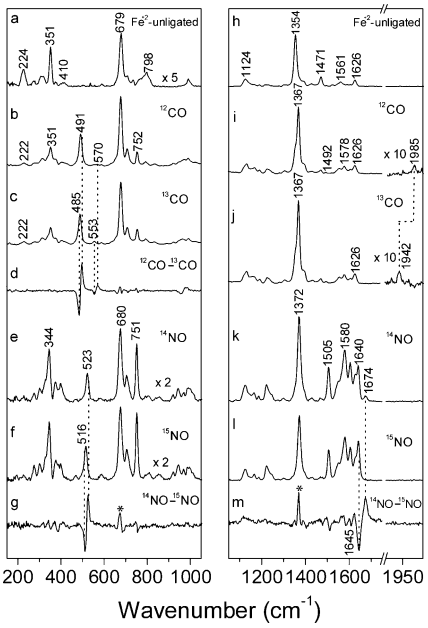

FIGURE 3: VCA0720 resonance Raman spectra: Fe^{2+} unligated in the low-frequency (a) and high-frequency region (h); ^{12}CO and ^{13}CO complexes and their difference spectra in the low-frequency (b—d) and high-frequency regions (i and j), respectively; ^{14}NO and ^{15}NO complexes and their difference spectra in the low-frequency (e—g) and high-frequency regions (k—m), respectively. The heme concentration was 17 μM. The subtraction factor in the isotopic difference spectra was adjusted to minimize features from vibrational modes that are insensitive to isotopic substitution. The asterisks indicate subtraction artifacts.

(B) NO Complexes. The NO complex of VCA0720 was also spectroscopically similar to sGC. Addition of NO to the Fe^{2+}-unligated protein resulted in a spectrum with a Soret band at ~399 nm, a decrease in the extinction coefficient, and a split α/β band. This spectrum is similar to that of sGC and indicates a 5-coordinate, NO complex. However, for *Tt*Tar4H, the addition of NO resulted in a spectrum with a Soret band at 420 nm and a split α/β band. This spectrum is similar to that of the 6-coordinate, NO complex from Hb (Table 1).

(C) O_2 Complex. *Tt*Tar4H forms a stable Fe^{2+}—O_2 complex. Fe^{2+}-unligated *Tt*Tar4H, contained in an anaerobic cuvette, was removed from the anaerobic chamber and exposed to air, and a spectrum was recorded. The spectrum exhibited a Soret band at 416 nm and a split α/β band. This spectrum is similar to that of oxy-Hb and suggests that *Tt*Tar4H forms a low-spin, Fe^{2+}—O_2 complex. The *Tt*Tar4H ferrous—oxy complex was very stable, exhibiting no spectroscopic changes overnight at 4 °C.

Resonance Raman Spectroscopy. Raman spectra of VCA0720 and *Tt*Tar4H are shown in Figures 3 and 4, respectively, and the data are summarized in Table 2 along with comparisons to sGC (*16*, *17*), Mb (*18*—*23*), and *Ax*PDEA1H (the heme domain of *Ax*PDEA1) (*24*).

(A) Fe^{2+}-Unligated Complexes. In the high-frequency region, the heme skeletal marker bands for VCA0720 and *Tt*Tar4H are observed, including the 1354 cm^{-1} ν_4 band that is sensitive to the heme oxidation state (*25*), the 1471 cm^{-1} ν_3 band, and the ν_2 bands (1561 and 1575 cm^{-1} for VCA0720 and *Tt*Tar4H, respectively). The ν_3 and ν_2 bands are sensitive to the spin and coordination state of the heme iron (*25*). The shoulder at 1374 cm^{-1} on the ferrous-unligated ν_4 peak at

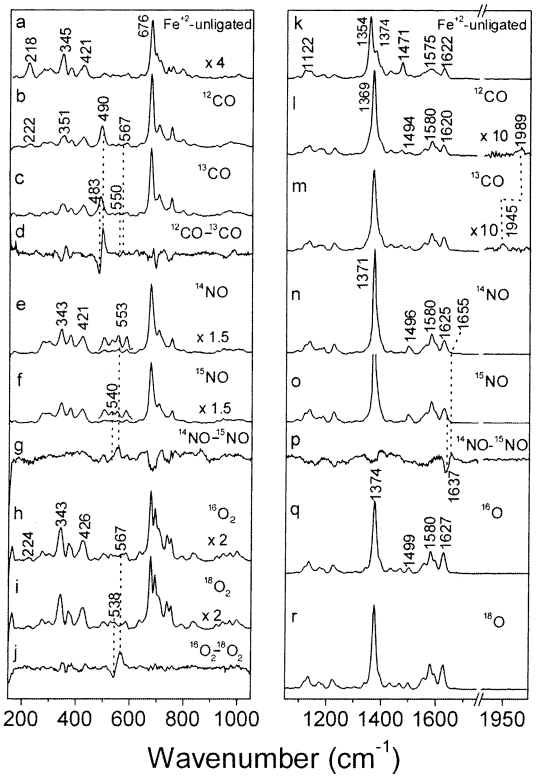

FIGURE 4: *Tt*Tar4H resonance Raman spectra: Fe^{2+} unligated in the low-frequency (a) and high-frequency region (k); ^{12}CO and ^{13}CO complexes and their difference spectra in the low-frequency (b−d) and high-frequency regions (l and m), respectively; ^{14}NO and ^{15}NO complexes and their difference spectra in the low-frequency (e−g) and high-frequency regions (n−p), respectively; $^{16}O_2$ and $^{18}O_2$ complexes and their difference spectra in the low-frequency (h−j) and high-frequency regions (q and r), respectively. The heme concentration was 47 μM. The subtraction factor in the isotopic difference spectra was adjusted to minimize features from vibrational modes that are insensitive to isotopic substitution.

Table 2: Heme Skeletal Vibrations and Vibrational Modes[a]

protein	ν_2	ν_3	ν_4	Fe−X	X−O	ref
Fe^{2+} unligated				ν(Fe−His)		
sGC	1562	1471	1358	204		*16, 17*
VCA0720	1561	1471	1354	224		this work
*Tt*Tar4H	1575	1471	1354	218		this work
Mb	1563	1471	1357	220		*18−23*
*Ax*PDEA1H	1557	1469	1354	212		*24*
CO bound				ν(Fe−CO)	ν(C−O)	
sGC	1583	1500	1371	472	1987	*16, 17*
VCA0720	1578	1492	1367	491	1985	this work
*Tt*Tar4H	1580	1494	1369	490	1989	this work
Mb	1587	1498	1372	512	1944	*18−23*
*Ax*PDEA1H	nr[b]	nr	nr	493	1973	*24*
NO bound				ν(Fe−NO)	ν(N−O)	
sGC	1584	1509	1375	525	1677	*16, 17*
VCA0720	1580	1505	1372	523	1674	this work
*Tt*Tar4H	1580	1496	1371	553	1655	this work
Mb	1584	1501	1375	554	1624	*18−23*
*Ax*PDEA1H	nr	nr	nr	560	1637	*24*
O_2 bound				ν(Fe−O)		
*Tt*Tar4H	1580	1499	1374	567		this work
Mb	1584	1507	1377	570		*18−23*
*Ax*PDEA1H	nr	nr	nr	567		*24*

[a] In cm^{-1}. [b] Not reported.

1354 cm^{-1} was due to incomplete exclusion of oxygen from the sample during the course of the experiment. However, the ν_3 band at 1471 cm^{-1} indicates ferrous unligated protein as the main sample component. The heme skeletal markers are similar to the corresponding bands in histidine-ligated, 5-coordinate, high-spin, Fe^{2+} hemoproteins such as sGC (Table 2). In the low-frequency spectrum, bands at 224 and 218 cm^{-1} are observed for VCA0720 and *Tt*Tar4H, respectively. These bands are assigned to the ν(Fe−His) stretching mode on the basis of previous observations that, in most histidine-ligated, Fe^{2+}−heme complexes, this stretching frequency is usually between 200 and 250 cm^{-1} (*26*), and that, in the NO and CO adducts, these bands are absent. On the basis of the above, both reduced proteins contain a 5-coordinate, high-spin heme.

(B) CO Complexes. The heme skeletal markers at 1369, 1494, and 1580 cm^{-1} are similar to the corresponding bands from histidine-ligated, 6-coordinate, low-spin, Fe^{2+} hemoproteins such as sGC (Table 2). In the low-frequency spectrum, isotope-sensitive bands at 491 and 490 cm^{-1} are observed for VCA0720 and *Tt*Tar4H, respectively. The predicted values for ^{13}CO isotopic frequencies are 485 cm^{-1} for VCA0720 and 484 cm^{-1} for *Tt*Tar4H. The observed frequencies of 485 and 483 cm^{-1}, respectively, are in excellent agreement. These bands are assigned to the ν(Fe−CO) stretching mode on the basis of their isotopic shift and their similarity to the ν(Fe−CO) frequency for *Ax*PDEA1H (493 cm^{-1}). In the high-frequency spectrum we observed isotope-sensitive bands at 1985 and 1989 cm^{-1} for VCA0720 and *Tt*Tar4H, respectively. The isotopic shifts also agree well with calculated values (calculated, 1941 and 1945 cm^{-1}, and actual, 1942 and 1945 cm^{-1}, for VCA0720 and *Tt*Tar4H, respectively). These bands are assigned to the ν(CO) stretching mode on the basis of their isotopic shift and their similarity to the reported ν(CO) frequency of 1987 cm^{-1} for full-length sGC as determined by FTIR. The CO isotopic sensitive vibration band at 979 cm^{-1} can be assigned to the first overtone of the ν(Fe−CO) stretching vibration. Like sGC, VCA0720 and *Tt*Tar4H have high ν(CO) stretching frequencies, and the 1989 cm^{-1} value observed for *Tt*Tar4H is the highest yet reported. Therefore, both proteins form CO complexes that are most similar to sGC: These complexes are 6-coordinate, low-spin and are notable for their high ν(CO) stretching frequency.

(C) NO Complexes. For the NO complex of VCA0720 (Figure 3), the high-frequency spectrum shows heme skeletal marker bands that are similar to the corresponding bands in 5-coordinate NO-sGC (Table 2). In the low-frequency spectrum, an isotope-sensitive band is observed at 523 cm^{-1}. The estimated ^{15}NO isotopic shift of about 7 cm^{-1} agrees well with the observed ν(Fe−NO) shift from 523 to 517 cm^{-1}. This band is assigned to the ν(Fe−NO) stretching mode on the basis of its isotopic shift and similarity to the ν(Fe−NO) frequency in sGC (525 cm^{-1}). We also observed an isotope-sensitive band in the high-frequency spectrum (1674 cm^{-1}). We estimate an isotopic shift value for $^{15}N-O$ stretching of about 27 cm^{-1}, which agrees well with our observation that the N−O stretch shifts from 1674 to 1645 cm^{-1}. On the basis of its isotopic shift and similarity to the ν(NO) frequency in sGC (1677 cm^{-1}), this band is assigned to the ν(NO) stretching mode. The NO complex of VCA0720 is, therefore, 5-coordinate and similar to sGC.

For *Tt*Tar4H (Figure 4), the high-frequency spectrum exhibits heme skeletal marker bands that are similar to the corresponding bands in 6-coordinate, low-spin NO-Mb. In

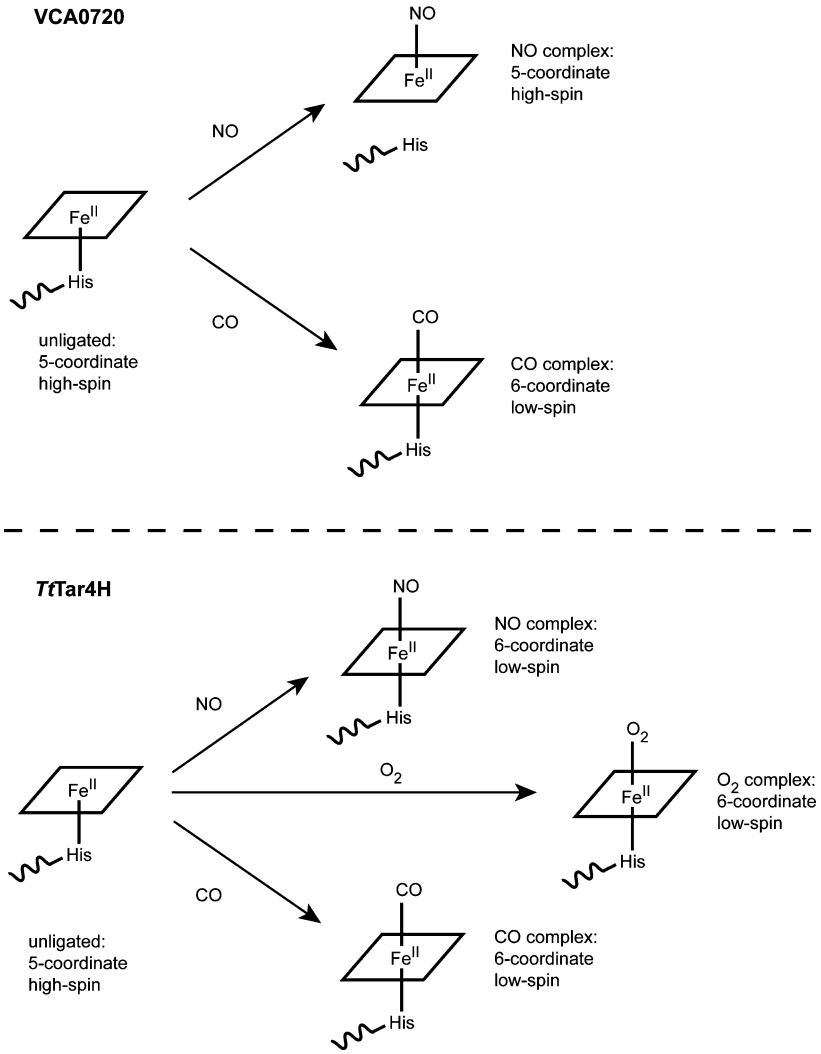

FIGURE 5: Summary of the results with VCA0720 and *Tt*Tar4H. A summary of the spectroscopic results is shown. VCA0720 forms stable complexes with NO and CO but not with O_2 and therefore has ligand-binding properties similar to those of the NO receptor soluble guanylate cyclase. *Tt*Tar4H, on the other hand, is isolated as a ferrous−oxy complex and has spectral properties similar to those of the globin family and, like the globins, forms stable complexes with NO and CO.

the low-frequency spectrum, bands in the 500−600 cm^{-1} region are weakly sensitive to isotopic substitution of the NO ligand. In particular, the 553 cm^{-1} band is plausibly attributed as the ν(Fe−NO) stretching mode based on its similarity to 6-coordinate Mb and NO-*Ax*PDEA1H (554 and 560 cm^{-1}, respectively). This band exhibits its sensitivity to $^{14}NO \rightarrow {}^{15}NO$ isotopic substitution, but the S/N ratio in the difference spectrum is insufficient to determine the shifted frequency. We estimate a ν(Fe−NO) frequency shift of 15 cm^{-1} upon ^{15}NO substitution. In the high-frequency spectrum, an isotope-sensitive band at 1655 cm^{-1} is observed. This band is assigned to the ν(NO) stretching mode on the basis of its isotopic shift (1637 cm^{-1}; calculated value 1625 cm^{-1}) and similarity to 6-coordinate *Ax*PDEA1H (1637 cm^{-1}). We conclude that *Tt*Tar4H forms a 6-coordinate, low-spin NO complex that is similar to *Ax*PDEA1H.

(D) O_2 Complex. For *Tt*Tar4H (Figure 4), the high-frequency spectrum exhibits heme skeletal marker bands that are similar to the corresponding bands in 6-coordinate, low-spin O_2-Mb. In the low-frequency spectrum, a single isotope-sensitive band at 567 cm^{-1} is observed. The predicted isotopic shift for the $^{18}O_2$−*Tt*Tar4H complex is 25 cm^{-1}, and the experimental value was 29 cm^{-1}. This band is assigned to the ν(Fe−O_2) stretching mode on the basis of its isotopic shift and similarity to the ν(Fe−O_2) frequency in *Ax*PDEA1H (567 cm^{-1}). *Tt*Tar4H forms an O_2 complex that is similar to *Ax*PDEA1H and is 6-coordinate and low-spin.

DISCUSSION

VCA0720 and TtTar4H Are Related to the Heme Domain of sGC. We assign VCA0720 and *Tt*Tar4H to the same family as the heme domain of sGC on the basis of the following similarities: First, both proteins have sequence homology to the heme domain of sGC (~20% identity). Second, sequence alignments with sGC reveal that specialized residues are conserved. For example, when compared to the rat β1 subunit, we find that His105 and a C-terminal Tyr-X-Ser-X-Arg (YSR) motif are conserved. His105 is the protein ligand to the heme cofactor in sGC, and a recent study has shown that the tyrosine and the arginine from the YSR motif are critical for heme binding (*27*). Finally, both of these proteins share spectroscopic properties with sGC. Like sGC, the Fe^{2+}-unligated forms of these proteins are 5-coordinate, high-spin, and the CO complexes are 6-coordinate, low-spin (Figure 5).

Divergent Ligand-Binding Properties. Although VCA0720, *Tt*Tar4H, and sGC have some common characteristics mentioned above, there are also some significant differences. First, we find different coordination states for NO: *Tt*Tar4H forms a 6-coordinate, low-spin NO complex like Mb while VCA0720 forms a 5-coordinate complex similar to sGC. Second, we find different reactivity toward oxygen: *Tt*Tar4H is able to form a stable ferrous−oxy complex while VCA0720, like sGC, does not. There are also more subtle differences as well. For example, although VCA0720 and *Tt*Tar4H have similar ν(CO) frequencies compared to sGC, their ν(Fe−CO) frequencies are moderately higher (491 and 490 cm^{-1} for VCA0720 and *Tt*Tar4H, respectively, compared to 472 cm^{-1} for sGC). sGC has one of the highest ν(CO) and lowest ν(Fe−CO) stretching frequencies, and on the basis of this observation, we have previously suggested that the distal pocket of sGC has significant negative polarity (*28*). This is based on the observation that the ν(CO) and ν(Fe−CO) frequencies are inversely correlated and are sensitive to distal pocket polarity (*29*, *30*). Negative polarity in the distal pocket can inhibit Fe $d_\pi \rightarrow$ CO π^* back-bonding, weakening the Fe−CO bond order and strengthening the C−O bond order. The moderately higher ν(Fe−CO) values for VCA0720 and *Tt*Tar4H suggest that their distal pockets may be different from sGC, possibly containing a hydrophobic environment rather than a negative one.

Lastly, we find varying ν(Fe−His) stretching frequencies (Table 2). VCA0720 and *Tt*Tar4H have higher frequencies that are closer to Mb (220 cm^{-1}) while sGC has an unusually low value (204 cm^{-1}). The ν(Fe−His) frequency is a direct measure of the Fe−His bond strength and is influenced by the proximal pocket environment (*26*). A weak bond is usually correlated with either the absence of a hydrogen bond to the histidine Nδ proton (less imidazolate character) or strain on the Fe−His bond that is induced by the protein. Both have been implicated in the weak Fe−His bond in sGC (*16*, *31*). The weak Fe−His bond in sGC (204 cm^{-1}) has also been implicated in its inability to form a stable ferrous−oxy complex (*32*), reflecting decreased electron density in the Fe d_π orbitals and less back-bonding to the O_2 π^* orbitals. The ability of *Tt*Tar4H to form a stable ferrous−oxy complex is consistent with its higher ν(Fe−His) frequency (218 cm^{-1}), which is similar to myoglobin (220 cm^{-1}). However, VCA0720 has a much stronger ν(Fe−His) frequency (224 cm^{-1}), and yet it does not bind oxygen, suggesting that, for VCA0720, distal effects may be an important determinant in the ability to exclude the formation of a stable ferrous−oxy complex.

It is likely that subtle differences in the proximal and distal pockets will be responsible for the variability seen in the Fe−His bond strengths, ν(Fe−CO) frequencies, NO coordination complexes, and ferrous−oxy complexes in the sGC-like heme domain family. This variation is consistent with a recent study of four different members of the heme−PAS domain family where significant differences in their heme coordination states, ν(Fe−His) frequencies, ligand-binding properties, and stretching frequencies were reported (*24*). This study, along with our findings here, raises an important question: If individual members of a heme domain family show significant variability in their ligand-binding properties and apparent function, then which features, if any, are invariant in individual family members; i.e., are there components that are completely conserved in every family member regardless of its individual function and ligand specificity? Sequence analysis of the sGC-like heme domain-containing family members reveals a conserved YSR motif that has been shown to be important for heme binding in sGC (*27*). We hypothesize that this motif will be part of a conserved core that is necessary for the function of this domain in all family members regardless of individual variations such as whether they bind O_2 or NO.

sGC-like Heme Domains That Discriminate between NO and O_2. What might our spectroscopic findings predict about the function of these prokaryotic proteins? Our data show that VCA0720 is similar to sGC, forming a 5-coordinate NO complex. In fact, the ν(NO) and ν(Fe−NO) stretching frequencies are almost exactly the same as sGC, indicating a very similar NO-bound pocket. In sGC, the formation of a 5-coordinate NO complex and the breaking of the Fe−His bond are thought to play a central role in activation of this enzyme (*33*). Furthermore, like sGC, VCA0720 is unable to form a stable $Fe^{2+}-O_2$ complex. sGC functions in an aerobic environment ($\sim$50 μM O_2) and has evolved to exclude oxygen binding in order to sense NO, which is present at much lower concentrations ($\sim$1 nM) (*34*, *35*). Thus, given these spectral similarities, it is likely that VCA0720 also acts as an NO sensor. VCA0720 and its prokaryotic orthologues are encoded in histidine kinase-containing operons. It is possible that VCA0720 binds NO and this NO−VCA0720 complex then regulates the operon-associated histidine kinase. NO, we speculate, could be derived from using NO_3^- as an electron acceptor when O_2 levels are low. NO then would serve as a signal for growth under low O_2 tension and could then regulate genes required for growth under these conditions using this operon.

*Tt*Tar4H, on the other hand, does form a stable $Fe^{2+}-O_2$ complex, which is similar to heme-bound O_2 sensors such as *Ax*PDEA1. This is the first report of the formation of a stable $Fe^{2+}-O_2$ complex in any protein from the sGC-like heme domain family. Because *T. tengcongensis* is a strict anaerobe, it seems likely that *Tt*Tar4H serves as an O_2 sensor. The *Tt*Tar4H heme domain comprises residues 1−188 of a predicted 602 amino acid protein. In the predicted protein, this heme domain is followed by a membrane-spanning region and then a methyl-accepting chemotaxis domain. We speculate that methylation of the MCP in response to O_2 binding serves as an initiating event in chemotaxis. It is tempting to speculate that *Tt*Tar4H and its orthologues, found only in strict anaerobes, function to sense O_2 and avoid this toxic environment.

The ν(Fe−O) frequency of *Tt*Tar4H at 567 cm^{-1} is close to that seen in Mb (570 cm^{-1}). In globins, differences in the ν(Fe−O) stretching frequencies have been attributed to differences in hydrogen bonding to the oxygen ligand. ν(Fe−O) frequencies in the region of 570 cm^{-1} are associated with stabilizing hydrogen bonds to the distal oxygen atom (*36*). The *Tt*Tar4H ν(Fe−O) frequency of 567 cm^{-1} is consistent with a stabilizing hydrogen bond that could enhance oxygen affinity (*36*−*38*).

In summary, VCA0720 and *Tt*Tar4H are hemoproteins that are related to the heme domain from sGC and are able to discriminate between NO and O_2. This conserved domain was previously named the HNOB domain (for *h*eme *n*itric *o*xide *b*inding domain), based solely on its sequence homol-

ogy to NO-sensing sGC (*11*). Our data suggest that this name does not adequately reflect the divergent ligand-binding properties of this domain and we, therefore, propose that this domain be named the H−NOX (*h*eme−*n*itric oxide/*ox*ygen binding) domain. Further analysis of the H−NOX domain is currently underway in order to understand molecular aspects of ligand discrimination and to establish its biological function.

ACKNOWLEDGMENT

We thank Chinmay Majmudar for help with the initial characterization of β1(1−194) and Dr. Elizabeth Boon for critical input and experimental expertise.

REFERENCES

1. Jain, R., and Chan, M. K. (2003) Mechanisms of ligand discrimination by heme proteins, *J. Biol. Inorg. Chem. 8*, 1−11.
2. Hou, S., Larsen, R. W., Boudko, D., Riley, C. W., Karatan, E., Zimmer, M., Ordal, G. W., and Alam, M. (2000) Myoglobin-like aerotaxis transducers in Archaea and Bacteria, *Nature 403*, 540−544.
3. Aono, S., Kato, T., Matsuki, M., Nakajima, H., Ohta, T., Uchida, T., and Kitagawa, T. (2002) Resonance Raman and ligand binding studies of the oxygen-sensing signal transducer protein HemAT from *Bacillus subtilis*, *J. Biol. Chem. 277*, 13528−13538.
4. Gilles-Gonzalez, M. A., Ditta, G. S., and Helinski, D. R. (1991) A haemoprotein with kinase activity encoded by the oxygen sensor of Rhizobium meliloti, *Nature 350*, 170−172.
5. Monson, E. K., Weinstein, M., Ditta, G. S., and Helinski, D. R. (1992) The FixL protein of Rhizobium meliloti can be separated into a heme-binding oxygen-sensing domain and a functional C-terminal kinase domain, *Proc. Natl. Acad. Sci. U.S.A. 89*, 4280−4284.
6. Chang, A. L., Tuckerman, J. R., Gonzalez, G., Mayer, R., Weinhouse, H., Volman, G., Amikam, D., Benziman, M., and Gilles-Gonzalez, M. A. (2001) Phosphodiesterase A1, a regulator of cellulose synthesis in Acetobacter xylinum, is a heme-based sensor, *Biochemistry 40*, 3420−3426.
7. Shelver, D., Kerby, R. L., He, Y., and Roberts, G. P. (1997) CooA, a CO-sensing transcription factor from Rhodospirillum rubrum, is a CO-binding heme protein, *Proc. Natl. Acad. Sci. U.S.A. 94*, 11216−11220.
8. Denninger, J. W., and Marletta, M. A. (1999) Guanylate cyclase and the NO/cGMP signaling pathway, *Biochim. Biophys. Acta 1411*, 334−350.
9. Zhao, Y., and Marletta, M. A. (1997) Localization of the heme binding region of soluble guanylate cyclase, *Biochemistry 36*, 15959−15964.
10. Stone, J. R., and Marletta, M. A. (1994) Soluble guanylate cyclase from bovine lung: Activation with nitric oxide and carbon monoxide and spectral characterization of the ferrous and ferric states, *Biochemistry 33*, 5636−5640.
11. Iyer, L. M., Anantharaman, V., and Aravind, L. (2003) Ancient conserved domains shared by animal soluble guanylyl cyclases and bacterial signaling proteins, *BMC Genomics 6*, 490−497.
12. Zhao, Y., and Marletta, M. A. (1997) Localization of the heme binding region in soluble guanylate cyclase, *Biochemistry 36*, 15959−15964.
13. Brandish, P. E., Buechler, W., and Marletta, M. A. (1998) Regeneration of the ferrous heme of soluble guanylate cyclase from the nitric oxide complex: acceleration by thiols and oxyhemoglobin, *Biochemistry 37*, 16898−16907.
14. Pan, D., Ganim, J. E., Kim, J. E., Verhoeven, M. A., Lugtenburg, J., and Mathies, R. A. (2002) Time-resolved resonance Raman analysis of chromophore structural changes in the formation and decay of rhodopsin's BSI intermediate, *J. Am. Chem. Soc. 124*, 4857−4864.
15. Di Iorio, E. E. (1981) in *Hemoglobins* (Antonini, E., Rossi-Bernardi, L., and Chiancone, E., Eds.) pp 57−71, Academic Press, New York.
16. Deinum, G., Stone, J. R., Babcock, G. T., and Marletta, M. A. (1996) Binding of nitric oxide and carbon monoxide to soluble guanylate cyclase as observed with resonance Raman spectroscopy, *Biochemistry 35*, 1540−1547.
17. Tomita, T., Ogura, T., Tsuyama, S., Imai, Y., and Kitigawa, T. (1997) Effects of GTP on bound nitric oxide of soluble guanylate cyclase probed by resonance Raman spectroscopy, *Biochemistry 36*, 10155−10160.
18. Choi, S., Spiro, T. G., Langry, K. C., Smith, K. M., Budd, D. L., and La Mar, G. N. (1982) Structural correlations and vinyl influences in resonance Raman spectra of protoheme comlexes and proteins, *J. Am. Chem. Soc. 104*, 4345−4351.
19. Tsubaki, M., and Yu, N. T. (1982) Resonance Raman investigation of nitric oxide bonding in nitrosylhemoglobin A and -myoglobin: detection of bound N−O stretching and Fe−NO stretching vibrations from the hexacoordinated NO-heme complex, *Biochemistry 21*, 1140−1144.
20. Hu, S., and Kincaid, J. R. (1991) Resonance Raman spectra of the nitric oxide adducts of ferrous cytochrome P450cam in the presence of various substrates, *J. Am. Chem. Soc. 113*, 9760−9766.
21. Tsubaki, M., Srivastava, R. B., and Yu, N. T. (1982) Resonance Raman investigation of carbon monoxide bonding in (carbon monoxy)hemoglobin and -myoglobin: Detection of Fe−CO stretching and Fe−C−O bending vibrations and influence of the quaternary structure change, *Biochemistry 21*, 1132−1140.
22. Takahashi, S., Ishikawa, K., Takeuchi, N., Ikeda-Saito, M., Yoshida, T., and Rousseau, D. L. (1995) Oxygen-bound heme-heme oxygenase complex: Evidence for a highly bent structure of the coordinated oxygen, *J. Am. Chem. Soc. 117*, 6002−6006.
23. Van Wart, H. E., and Zimmer, J. (1985) Resonance Raman evidence for the activation of dioxygen in horseradish oxyperoxidase, *J. Biol. Chem. 260*, 8372−8377.
24. Tomita, T., Gonzalez, G., Chang, A. L., Ikeda-Saito, M., and Gilles-Gonzalez, M. A. (2002) A comparative resonance Raman analysis of heme-binding PAS domains: heme iron coordination structures of the BjFixL, AxPDEA1, EcDos, and MtDos proteins, *Biochemistry 41*, 4819−4826.
25. Spiro, T. G., and Li, X.-Y. (1988) in *Biological Applications of Raman Spectroscopy* (Spiro, T. G., Ed.) pp 1−37, John Wiley & Sons, New York.
26. Kitagawa, T. (1988) in *Biological Applications of Raman Spectroscopy* (Spiro, T. G., Ed.) pp 97−131, John Wiley & Sons, New York.
27. Schmidt, P. M., Schramm, M., Schroeder, H., Wunder, F., and Stasch, J. P. (2004) Identification of residues crucially involved in the binding of the heme moiety of soluble guanylate cyclase, *J. Biol. Chem. 279*, 3025−3032.
28. Kim, S., Deinum, G., Gardner, M. T., Marletta, M. A., and Babcock, G. T. (1996) Distal pocket polarity in the unusual ligand binding site of soluble guanylate cyclase: implications for control of •NO binding, *J. Am. Chem. Soc. 118*, 8769−8770.
29. Cameron, A. D., Smerdon, S. J., Wilkinson, A. J., Habash, J., Helliwell, J. R., Li, T., and Olson, J. S. (1993) Distal pocket polarity in ligand binding to myoglobin: deoxy and carbonmonoxy forms of a threonine68(E11) mutant investigated by X-ray crystallography and infrared spectroscopy, *Biochemistry 32*, 13061−13070.
30. Li, T., Quillin, M. L., Phillips, G. N., Jr., and Olson, J. S. (1994) Structural determinants of the stretching frequency of CO bound to myoglobin, *Biochemistry 33*, 1433−1446.
31. Schelvis, J. P., Zhao, Y., Marletta, M. A., and Babcock, G. T. (1998) Resonance Raman characterization of the heme domain of soluble guanylate cyclase, *Biochemistry 37*, 16289−16297.
32. Zhao, Y., Schelvis, J. P. M., Babcock, G. T., and Marletta, M. A. (1998) Identification of histidine-105 in the β1 subunit of soluble guanylate cyclase as the heme proximal ligand, *Biochemistry 37*, 4502−4509.
33. Zhao, Y., Brandish, P. E., Ballou, D. P., and Marletta, M. A. (1999) A molecular basis for nitric oxide sensing by soluble guanylate cyclase, *Proc. Natl. Acad. Sci. U.S.A. 96*, 14753−14758.
34. Malinski, T., Taha, Z., and Grunfeld, S. (1993) Diffusion of nitric oxide in the aorta wall monitored in situ by porphyrinic microsensors, *Biochem. Biophys. Res. Commun. 193*, 1076−1082.
35. Malinski, T., and Taha, Z. (1992) Nitric oxide release from a single cell measured in situ by a porphyrinic-based microsensor, *Nature 358*, 676−678.
36. Rousseau, D. L., and Friedman, J. M. (1988) in *Biological Applications of Raman Spectroscopy* (Spiro, T. G., Ed.) pp 133−215, John Wiley & Sons, New York.
37. Walters, M. A., Spiro, T. S., Suslick, K. S., and Collman, J. P. (1980) Resonance Raman spectra of (dioxygen)(porphyrinato)-

(hindered imidazole)iron(II) complexes: Implications for hemoglobin cooperativity, *J. Am. Chem. Soc. 102*, 6857−6858.
38. Das, T. K., Couture, M., Ouellet, Y., Guertin, M., and Rousseau, D. L. (2001) Simultaneous observation of the O- - -O and Fe- - -O_2 stretching modes in oxyhemoglobins, *Proc. Natl. Acad. Sci. U.S.A. 98*, 479−484.

BI049374L